Supernova-induced processing of interstellar dust in a turbulent, magnetized and high-density ISM.

Aurora Capobianco

University of Bath, Claverton Down, BA2 7AY Bath, United Kingdom;
Nordita, Albanova, Hannes Alfvéns väg 12, 114 19 Stockholm, Sweden

Email: ac2809@bath.ac.uk

Abstract. The overall structure and dynamics of the interstellar medium (ISM) are governed largely by the outflow of energy from evolved stars. The forward shock driven by a supernova (SN) plays an essential role in the injection of momentum into the ISM, altering the structure, chemistry and dynamics of potential star-forming material such as dust grains. A persistent dilemma in the field of interstellar dust research involves the large discrepancy between the timescales for dust formation from late-stage stars and its seemingly more rapid destruction within interstellar shocks. A full 3D treatment of a blast wave propagating through an inhomogeneous, turbulent ISM is performed onto a high-density region reproducing a dense clump in a molecular cloud. The purpose of this investigation is to quantify the impact of ambient gas and dust density on the cleansing effect of a SN on surrounding dust particles. The magneto-hydrodynamic simulations are run with initial conditions emulating a realistic ISM and post-processing calculations include dust processing due to ion sputtering, accretion, and grain–grain collisions. The model exhibits a decreased efficiency in the blast wave expansion and consequently constrains the dust processing, resulting in low accumulated dust loss compared to previous simulations at a lower ISM density.

1. Introduction

Galactic objects are embedded in the interstellar medium (ISM), a dynamic environment critical to galaxy evolution. The ISM is known to be magnetized, which is explained by dynamo action, the process of converting turbulent kinetic energy to magnetic energy [1]. The grand design of galaxies is explained by large-scale dynamos, but small-scale dynamo (SSD) action is also a contributor to the magnetic field dynamics in the ISM [2]. Turbulence is believed to be responsible for the amplification and maintenance of comic magnetic fields via the SSD mechanism, and it is driven by several mechanisms including stellar outflows, supernova explosions, and gravitational instabilities [3].

The ISM is affected by the injection of mass in the form of dust grains, made of mostly silicates and carbonaceous material from evolved stars and supernovae (SNe). Cosmic dust is no longer perceived solely as an impediment to the observational study of stars and galaxies, but it is now acknowledged as an integral contributor to the evolution and current state of the Universe. The most evident effect of dust grains is that they cause the extinction of starlight, meaning that they act as coolants, affecting and facilitating the dynamical and thermal evolution of the gas in star formation [4]. Despite advancements in our understanding of the chemical properties of cosmic dust [5] and its role in interstellar space, there are several areas where our understanding remains limited. The physics of grain aggregation is a topic of great interest and intensive experimental and theoretical research because it is the initial step toward planet formation [6], while the physical form of the dust grains and their survivability in shocks is

challenging to quantify or simulate. As has been recognized for many years [7], the dominant mode of destruction occurs through fast shock waves, predominantly originating due to SN explosions.

1.1. Impact of shocks on dust grains

A shock wave is a supersonic, pressure-driven structure that leads to impulsive heating of the shocked gas [8]. Behind a shock front, charged grains are accelerated by the Lorentz force which causes a gyromotion of the grains around the magnetic field lines [9], and by collisional and plasma drag [10] as the post-shock gas cools and compresses. Grain processing occurs because of the acceleration of the grains and the compression and heating of the gas. Dust growth processes include gas accretion, ion trapping and coagulation [4].

The main processes that lead to dust destruction are shattering and vaporisation caused by grain-to-grain collisions, which regulate the size distribution of the dust. Collisions in the ISM may result in fragmentation or aggregation, depending on the impact speeds of the colliding particles [12]. For large collision velocities, dust can be fully vaporized, which means that the whole material goes into the gas phase [13]. Intermediate impact speeds result in shattering of the dust grains and partial vaporisation and at low collision velocities, the grains are not shattered but bounce or merge.

Sputtering is the removal of grain atoms after the bombardment of gas particles and is considered to be the primary dust destruction mechanism in SN-generated shock waves [14]. The compression in the shock, with the accompanying enhancement of the magnetic field, acceleration of the grains and heating of the gas act to enhance the sputtering of the grains [15]. Sputtering of a dust grain can be distinguished between thermal, arising from the kinetic motion of atoms or ions in heated gas, or non-thermal in cases where gas and dust are in rapid relative motion [16]. Shock-driven grain–grain collisions modify the size distribution by shattering, thereby increasing the surface area exposed to erosion which results in the vaporisation and fragmentation of grains [17]. The extent of shock heating and the accumulation of gas within the remnant shell are crucial factors influencing the rates of grain-grain collisions and sputtering [14,15]. Further dust growth processes like gas accretion or ion trapping [18] of destroyed dust material only play a minor role.

1.2. Tackling the dust-budget crisis

Interstellar dust research faces a controversy regarding the dust abundance in the ISM, as a consequence of the timescales for dust formation from late-stage stars exceeding those of dust destruction within interstellar shocks [19]. Dust abundances in high-redshift galaxies appear to exceed theoretical predictions, given expected rates of dust destruction [20, 21]. Previous research [14] has shown that in a SN shock, silicate grains are seemingly more resilient than carbonaceous grains, but the destruction lifetime found is short compared to the dust injection timescale. As Bocchio et al. [14] suggest, these results imply that the re-formation or survival of dust grains in denser regions of the ISM must be efficient to match the observations, since silicate re-formation under a low temperature and density ISM seems to be problematic [19].

For this reason, shocks into dense clumps are of particular interest. If a SN is located in a diffuse ambient medium, its impact remains fairly limited, and only a small percent of the momentum is given to the gas. When a SN explodes inside a dense molecular cloud, up to one-half of the momentum can be given to the gas, which suggests that these events influence the dust dynamics greatly [22]. Molecular clouds are turbulent and strongly affected by stellar feedback [23] and are known to harbour large populations of binaries. The bulk of binaries is a consequence of the high stellar densities found in molecular clouds, meaning that dynamical interactions that create or alter binaries occur frequently, and the increased mass of these systems causes them to sink to the centre of the cloud, where encounter rates are maximized. It is therefore reasonable to expect that SN progenitors will be enhanced in high-density regions of molecular clouds, providing further motive to consider the effects of SN blast waves in a dense medium.

Previous hydrodynamic simulations [24] have investigated the effects of a SN blast wave expanding in a uniform and modestly perturbed ISM on dust transport, dust destruction, and grain growth.

Outcomes (for $n = 0.1$ cm^{-3} and $n = 1$ cm^{-3}, where n is the gas density), have confirmed that the ambient ISM gas density determines the reach of an SN blast wave and the size of the affected portion of the ISM as theorized in [7]. The inclusion of shattering due to grain-grain collisions in the dust processing model resulted in an increase in the predicted dust cleansing efficiency, against the observed dust abundances in starburst galaxies [20]. Although magnetic field effects had not been included in the models, decaying dusty magneto-hydrodynamic (MHD) turbulence simulations [25] have shown that the gas-grain coupling provided by the Lorentz force offers grains relative protection from shattering. Gent et al. [11] derived criteria for the appearance of an SSD in simulations of interstellar turbulence and confirmed that an SSD is easily excited by ISM turbulence, a result that appears to converge at resolutions below 1 pc [2].

Our understanding of how MHD turbulence influences the dynamics and survival of charged dust particles is limited. To quantify magnetic field effects on the phenomenon, the same dust processing models have been applied to turbulent MHD simulations [26]. The Lorentz force has been shown to have strong effects on the rate of dust destruction, halving the dust loss under the same conditions. Dust survival due to magnetic effects can vary according to the distribution of the ISM gas, its mean density, and the ambient dust abundances at the site of the SN.

In this paper, we study the same dust processing models in a medium of average gas density of 20 cm^{-3} reaching a peak density of 400 cm^{-3}, henceforth requiring increased model resolution for the system to be resolved. The elevated density allows us to observe the effects of the blast wave in a region with properties comparable to those of a dense clump of gas and dust inside a molecular cloud. MHD simulations with the PENCIL CODE [27] are used to model the expansion of the SN in a turbulent multiphase ISM, and post-processing simulations with the PAPERBOATS [28] code are used to model the dust transport as well as grain destruction and growth processes in the medium.

2. Methods

In this work, gas and dust are treated as dynamically separate fluids. This section outlines the physical ingredients of the models, including our basic equations, initial and boundary conditions, and adaptations applied to the simulations.

2.1. Numerical simulations

The simulations of the dust are applied to a background ISM gas modelling the MHD of the explosion of a SN. The MHD turbulence of the ambient ISM and its further evolution is derived by solving numerically a set of MHD equations for a non-ideal, compressible gas using the PENCIL CODE [27]. The code is designed for fully non-linear, compressible MHD equations, and the full description of the system is given by [11]. The PENCIL CODE is highly modular and can easily be adapted to a large variety of physical setups and it is designed for efficient computation with massive parallelization [1, 29]. The third-order Runge-Kutta-Fehlberg adaptive time step method is implemented, which limits the estimated local error relative to second order to select an optimal step size.

Here follows a description of the steps taken to obtain the required MHD simulation.

2.1.1. Modelling supernova-driven turbulence. As a starting point for our simulation, we employ a snapshot representing a statistical steady state derived from a three-dimensional MHD simulation of SN-driven turbulence [11]. The domain of the model is defined by a periodic Cartesian cube of length 256 pc with a grid resolution size of 0.5 pc. A weak random magnetic field is amplified by SNe explosions randomly located in an initially homogeneous ISM. Each event injects 10^{51} erg of thermal energy and occurs at a Poisson rate of approximately 1 Myr^{-1}, equivalent to about 20% of the solar neighbourhood rate, which maintains a multiphase ISM [30]. SNe shock fronts compress and amplify the magnetic field, resulting in a strong local and almost instantaneous correlation between the field and density. However, the turbulence resulting from the sporadic heating and interactions of the SN remnants drives an SSD. The SSD induces rapid amplification of the magnetic field independently of the gas density reducing the correlation of magnetic energy to gas density [11].

The SN-driven turbulence model excludes large-scale magnetic field dynamics by omitting global-scale rotation, shear, and stratification [11]. Using the dynamo-generated magnetic field yields a more reliable structure related to the gas flow and thermal properties than adding a random field or one correlated to the gas density. As described in [31], non-adiabatic radiative cooling [32] and UV heating processes are included in the simulation, but the effects of self-gravity are neglected due to the Jeans length exceeding the size of the domain [26].

2.1.2. Remeshing. Within the domain, a high-density region of diameter 5 pc is chosen as an optimal site for the SN injection. The domain is rotated and shifted so that the high-density region would coincide with the centre of the grid. This process aims at obtaining a domain of 512^3 cells of size 0.125 pc compared to the initial 0.5 pc, with a resultant size of the grid equal to 64 pc (see Table 1). The process of remeshing involves the adaptation of a previously written code included in the PENCIL CODE package, `remesh.py`, created to increase the resolution of a chosen simulation by using linear interpolation. The original code was designed to generate a new simulation starting from a source simulation, resulting in a domain of a larger amount of cells depending on the required scaling factor. To achieve a resolution of 0.125 pc the interpolation would have developed a grid of 2048^3 cells (with a multiplying factor of 4), which would have been computationally too expensive to use for the ISM evolution. The code is hence adapted to select the necessary chunks of the source data cube before performing the interpolation. At this stage, a cube of size 134^3 cells corresponding to 67 pc in length is extracted out of the original 512^3 cells. The volume is delineated by imposing as its centre the location of maximum density and selecting $64 + 3$ cells in every direction. The 3 additional cells represent the ghost zones used to implement boundary conditions, initially set to periodic. These form three outer grid planes that allow derivatives at the boundary to be calculated in the same way as at interior grid points. The interior values of the variables are used to specify their ghost zone values [31].

The data cube is interpolated, producing a grid of size 64 pc with an enhanced resolution of 0.125. The initial simulation had a total mass enclosed in the domain fixed to 6×10^4 $M_\odot$. Consequently, the remeshing process outputted a domain with the same amount of mass, resulting in the mean density increasing from 1 to about 40 cm^{-3}, with a peak density of 1500 cm^{-3}. The peak density of this model exceeds the requirements for our investigation, leading us to half the total enclosed mass which results in a maximum density of 400 cm^{-3}. The boundaries are changed so that the mass does not have to be conserved, allowing for inflows and outflows and the velocity field is corrected to maintain the momentum and avoid spikes in the velocity. Alternatively, the kinetic energy density could be conserved by reducing the velocity by $\sqrt{2}$ as conserving momentum reduces the overall energy.

For our study of a single SN expansion, the periodic boundary conditions of the original model are no longer valid. When a sharp structure approaches a boundary, the strong gradients can lead to artefacts in the ghost zones that affect the interior. In some cases, a high shock with extremely high temperature and very low gas density would appear close to the boundary due to unmatching boundary conditions between the source and new simulation, resulting in the time step collapsing to a value smaller than 10^{-5} yr. All components of velocity are set to a vanishing first derivative, permitting gas flow across the boundary in both directions, but ensuring that the flow is dominated by the interior dynamics. To prevent an artificial enhancement of temperature spikes or gas density drops in the ghost zones, temperatures and densities are kept equal to their values at the boundary. These boundary conditions allow gas to escape without preventing inward flows, and for the magnetic vector potential $\boldsymbol{A}$ we adopt an anti-symmetric condition such that:

$$\begin{aligned} \delta^2 \boldsymbol{A}_x/\delta^2 x \;&=\; \delta \boldsymbol{A}_y/\delta x = \delta \boldsymbol{A}_z/\delta x = 0 \\ \delta \boldsymbol{A}_x/\delta y = \delta^2 \boldsymbol{A}_y/\delta^2 y \;&=\; \delta \boldsymbol{A}_z/\delta y = 0 \\ \delta \boldsymbol{A}_x/\delta z \;=\; \delta \boldsymbol{A}_y/\delta y &=\; \delta^2 \boldsymbol{A}_z/\delta^2 z = 0, \end{aligned}$$

producing a nearly uniform magnetic field near the boundary. It is important to formulate boundary conditions that admit the flow of matter and energy while minimising any associated artefacts that might

affect the interior. These boundary conditions could eventually lead to the loss of gas and energy, but over a long term and sufficiently far from the SN location so as not to affect the analysis of the remnant.

Kirschlager et al. [26] found that the initial correlation of dust to gas used in the PAPERBOATS reaches an alternative equilibrium within $20 - 50$ kyr, so to obtain a more realistic distribution of dust prior to the SN injection we now delay the explosion. The simulation evolved for 100 kyr to ensure that the system reached a relaxed state.

2.1.3. Simulating the SN blast wave. At the time at which we apply the interpolation process to this simulation, we cease the continuous random SN explosions, to first increase the resolution of the model, and then isolate the effects during the lifespan of the single SN remnant. The single SN is modelled by injecting 10^{51} erg of thermal energy with spherical Gaussian profile of radius 2 pc on a grid point located in the centre of the domain. In the highly dynamic and inhomogeneous ISM the properties of the expansion phase of the remnant do not converge to the ideal analytic solutions of Sedov-Taylor as described in [33]. The energy injection is applied in a single time step at $t = 100$ kyr and any additional mass from the SN ejecta is negligible and thus omitted. The initial condition creates a blast wave, which rapidly evacuates the ISM from the origin of the sphere and continues to expand into the ambient ISM. The SN explosion has been considered in a dense region of $n_{\mathrm{centre}} = 350$ cm^{-3} (Sim A), compared to previous simulations [26] that used $n_{\mathrm{centre}} = 0.7$ cm^{-3} (Sim B) and $n_{\mathrm{centre}} = 0.03$ cm^{-3} (Sim C) (see Table 1) in a more diffuse region of the ISM.

Table 1. Properties and outcomes of the simulations

	n_{avg} (cm^{-3})	n_{centre}[1] (cm^{-3})	Box length (pc)	Resolution (pc)	Accumulated dust losses ($M_\odot$)		
					5 kyr	25 kyr	50 kyr
Sim A	20	350	64	0.125	12	12	12
Sim B	1	0.7	256	0.5	1	12	14
Sim C	0.1	0.03	256	0.5	0	0.3	1

[1] Indicates the typical gas number density of the explosion epicentre at $t_{\mathrm{SN}} = 0$.

2.2. Dust processing

We employ the post-processing software PAPERBOATS [28] to examine the evolution of dust in turbulent ISM gas upon encountering a SN shock wave. The software utilizes the temporally and spatially resolved data for gas density, velocity, temperature and magnetic field obtained from the PENCIL CODE to calculate the spatial distribution of the dust particles. While PAPERBOATS is capable of handling 3D simulations, we limit our analysis to the central slice along the middle of the PENCIL CODE's output (a single cell in the z-direction). This decision is made to manage the substantial computational demands associated with highly resolved 3D post-processing. Snapshots of the simulation are taken at constant intervals of 100 yr, from $t = 50$ kyr until $t = 550$ kyr, resulting in 5000 snapshots. In the model, we assume an initial dust abundance proportional to the gas density. The dust location is discretized to spatial cells in the domain, using the so-called 'dusty-grid approach'. The

dust grains are assumed to be compact, homogeneous and spherical. A detailed description of the modelling and parameters of dust transport, sputtering, and grain–grain collisions is given in Sections 4.4–4.6 in [28].

Initially, the dust is at rest distributed in the domain with constant gas-to-dust mass ratio set to $\Delta_{\mathrm{gd}} = 100$, which corresponds quite well with what we know about the ISM [34]. The ratio is homogeneous throughout the domain everywhere at $t_{\mathrm{dust}} = 0$, then becomes inhomogeneous because the destruction effects are different at each point in the domain. Here, t_{dust} indicates the time passed after the dust processing started, from the initial snapshot at $t = 50$ kyr from the MHD simulation.

The grains in our simulations are made of silicate material, with a grain size distribution of type MRN [35]. The initial grain-size distribution follows a power-law $a^{-\gamma}$ with index $\gamma = 3.5$ with absolute values for the minimum and maximum grain radius defined as $a_{\mathrm{min}} = 0.6$ nm and $a_{\mathrm{max}} = 250$ nm. Dust processing can produce grains that are smaller or larger than the dust grain sizes defined in the initial distribution. Dust material with sizes below a_{min} is treated as destroyed and is assigned to the gas phase. Due to the nature of the post-processing, the dust medium cannot alter the state of the surrounding gas medium and no feedback is considered. These effects can be regarded as negligible in this context.

We observe the dust transport in the medium and calculate the cumulative dust losses $M_{\mathrm{destr.dust}}$ and the amount of gas mass cleared of dust, defined as $M_{\mathrm{cl.gas}} = \Delta_{\mathrm{gd}} \times M_{\mathrm{destr.dust}}$ [36].

3. Results

3.1. Evolution of the MHD model

We have performed simulations of an SN blast wave expanding in a 3D domain using the PENCIL CODE [27] as described in Section 2.

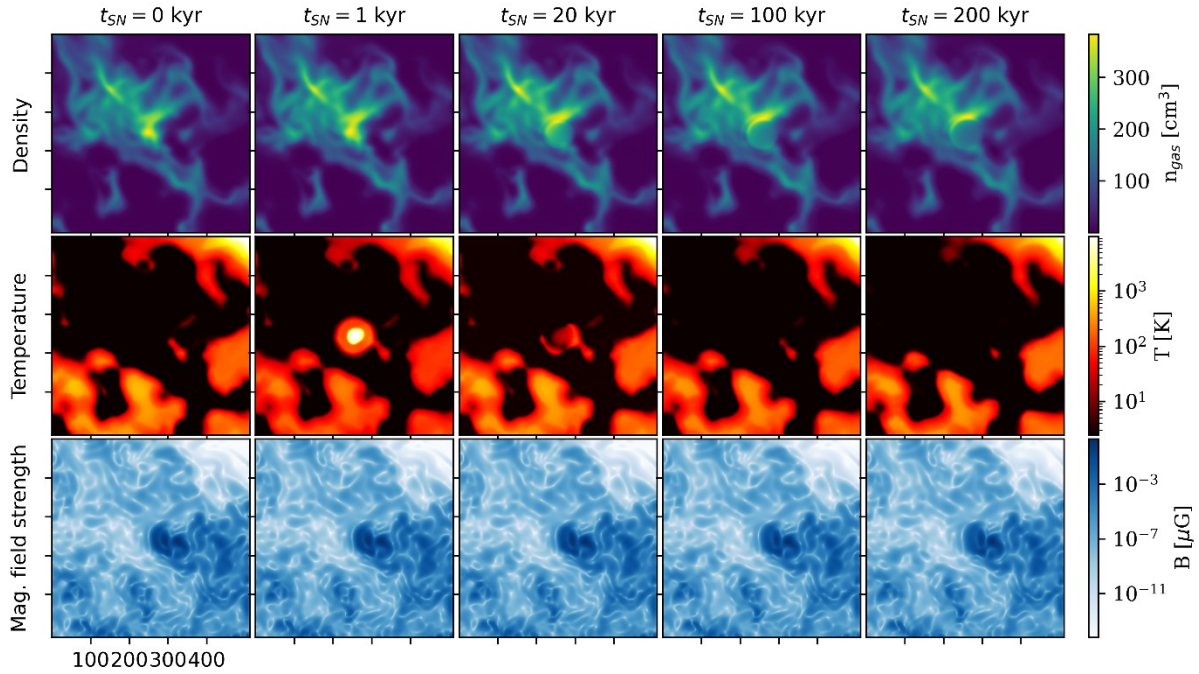

Figure 1. Temporal evolution of the gas density, temperature and magnetic field strength in the turbulent medium, taken from a slice through the middle of the simulation box in the xz-plane. Here, t_{SN} indicates the time passed after the SN injection.

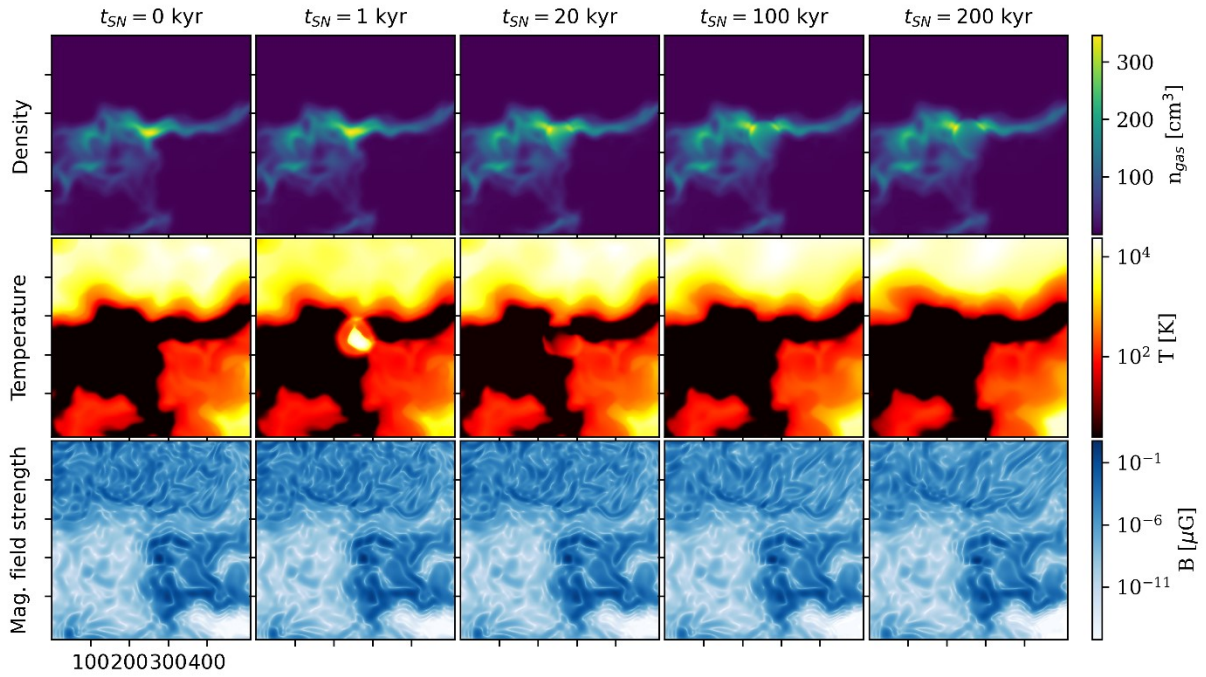

Figure 2. Temporal evolution of the gas density, temperature and magnetic field strength in the turbulent medium, taken from a slice through the middle of the simulation box in the xy-plane.

Figures 1 and 2 show different planes of the evolution of the blast wave propagating through the turbulent and inhomogeneous ISM gas. The first row depicts a slice of the projected linear density, with the blast wave being visible after a few kyr and reaching a shell size of about 10 pc across at $t_{\mathrm{SN}} = 200$ kyr. Corresponding temperatures are illustrated in the middle row. The temperature profile of the remnant retains a signature of its self-similar spherical origins until 1 kyr after the injection, but the subsequent heat expansion is irregular due to the multiphase ISM structure. At $t_{\mathrm{SN}} = 100$ kyr there is no signature of the SN in the temperature profile, due to high radiative losses from cooling in the dense medium reducing the strength of the blast wave early on.

In this model reverse shocks are weaker and damped more rapidly by its relatively higher density remnant interior. The lower row displays the magnetic field strength. In the dense remnant, the magnetic field strength seems almost unaffected, showing some slight outflows on the top right of the xy-plane (Figure. 2) only after $t_{\mathrm{SN}} = 100$ kyr. Furthermore, the magnetic field strength results to be much weaker than the expected mean of about 0.01 μG. When simulating the ISM, the initial magnetic field has a maximal magnitude of order 0.5 μG. The saturation of the dynamo is about 5% equipartition due to the absence of a mean-field and mean-field dynamo, so is about 10th the strength we might anticipate in the actual ISM [11].

The simulation is stopped after $t_{\mathrm{SN}} = 450$ kyr from the SN injection as the SN had cooled to the background temperature. Compared to previous simulations [24, 26] the run time has been reduced significantly but it has been taken into account that the blast wave speed is highly affected by the density of the medium. The blast wave does not reach the domain edges because of the high density of the medium, resulting in a slow evolution with a maximal blast wave speed of 100 km/s.

3.2. Dust destruction effect of the blast wave

In Figure 3 we illustrate the evolution of the dust component from the post-processing runs with PAPERBOATS. The first few kyr are critical to the effect of ambient gas density at the SN epicentre on total dust destruction. The dense explosion epicentre is impacted very quickly by the blast wave. Dust

grains in the central region are either swept or destroyed by the blast wave through sputtering, fragmentation or vaporisation. The dust densities show significant alteration, especially for larger dust

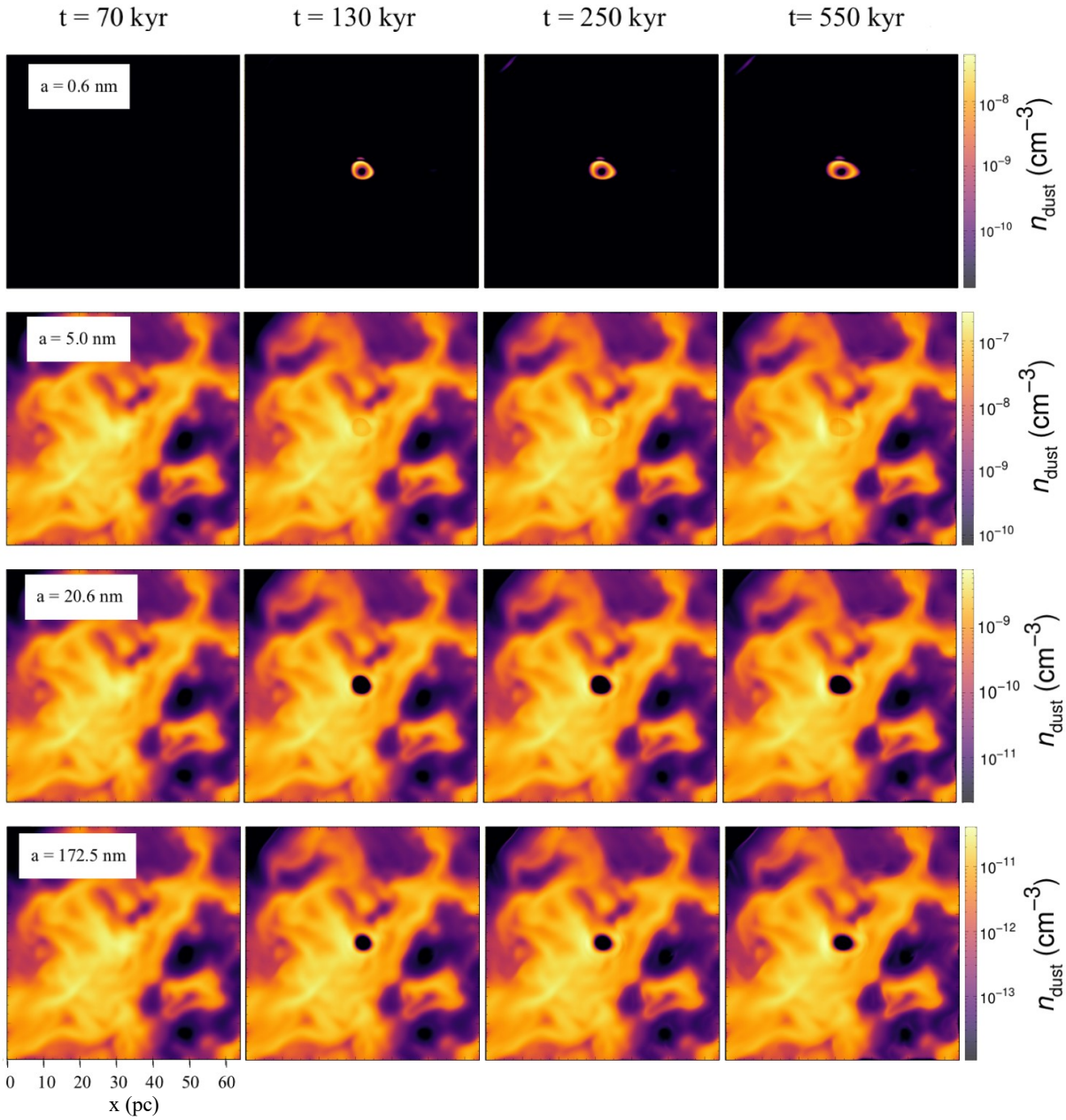

Figure 3. Temporal evolution of the spatial dust density when the SN explodes in the high-density region. The rows show the distribution of 0.6, 5, 20.6, and 172.5 nm grains, respectively. Note that the density scale varies between rows and the length scale is indicated in the lower left panel. Here t represents the time from the start of the MHD simulation, the SN is injected at $t = 100$ kyr.

grain sizes $a > 20$ nm. Destruction has a reduced impact on grains of size $a = 5$ nm (see second row, Figure 3), and the smallest grain sizes (0.6 nm, first row) are not included in the initial distribution but result from shocks and turbulence fragmenting and sputtering larger grains.

Most of the dust destruction occurs within 1.79 kyr from the SN injection, with a total percentage mass loss $\eta = M/M_0 = 2\%$. This corresponds to $M_{\mathrm{destr.dust}} = 12$ M$_\odot$ and therefore $M_{\mathrm{cl.gas}} = 1200$

$M_\odot$. This remains almost unchanged as the simulation evolves, the affected area develops slowly and is constrained to less than 10 pc across by the end of the simulation.

Due to ambient turbulence, the dust processing continues outside the remnant. In order to calculate the dust processing associated with the remnant and distinguish it from the effect of the ISM turbulence, the same dust processing model can be applied to a MHD simulation without the SN explosion. The background processing provides a dust destruction fraction by pure turbulence.

4. Discussion

Compared to previous simulations [24, 26, 31, 37], the temperatures of the slices in Figures 1 and 2 show a lack of hot gas in the remnant. However, in the slice immediately after the explosion, a region of 10^6 K gas is found. Due to the very high gas density, the ISM cools much more rapidly. Typical ISM simulations evolve with a minimum cooling time of around 10 yr [11]. With the very high density, the cooling time could be as short as 1 yr, meaning that the gas cools by 1 K every $1/e$ yr [38]. Kim & Ostriker [39] identified conditions for including momentum injection to obtain the snowplough solution in a dense gas at low resolution. Here we have enough resolution, but might need to consider a smaller injection radius to enhance the temperature and pressure gradient and evacuate the core more efficiently.

The initial condition has the cloud surrounded by a hot diffuse ISM, which does not cool as quickly as the remnant inside the dense structure. The mean magnetic field strength was expected to be around 0.01 μG, but the field decayed too quickly. This could be a consequence of the resistivity being too low, affecting the rate of decay. Due to the slow and inhibited SN blast wave expansion, the dust processing results are limited. Theoretically, the dust-mass fraction being destroyed increases with the amount of dust initially present in the ISM [40]. In our simulation (Sim A), the mass loss had reached 12 $M_\odot$ by $t_{SN} = 2$ kyr, while in Sim B only about 1 $M_\odot$ was destroyed within the first 5 kyr after the explosion. The background processing of dust is likely to be significant, as demonstrated in [26]. The only route to obtain the net effect of the blast wave is to compare the dust destruction fractions between simulations with and without SN.

Further investigation is required to understand the impacts of shocks in a magnetized high-density medium. Both [25] and [26] have shown that magnetic pressure provides extra support against the shell compression and therefore reduces non-thermal sputtering. In [25], simulations with and without Lorentz forces on dust grains were performed, concluding that charged grains of large size ($1 - 2$ μm) in this environment are significantly better coupled to the gas than uncharged grains and marginally less likely to undergo shattering. Kirschlager et al. [26], show in their Figure 4 the total dust mass and cleared gas mass as a function of time. When comparing results between models with and without Lorentz forces, a reduction in the fragmentation of large grains as the SN evolved was found.

For our investigation the dust composition is assumed to be pure silicates, but with PAPERBOATS it is also possible to consider pure graphite or a mixture of Si and C which would be more congruent to the observed composition [5]. A new approach to calculate dust vaporisation in grain-grain collisions allowed us to consider partial grain vaporisation (see section 4.5 in [41]), while in previous simulations [24, 26] only total vaporisation was considered. The effects of this implementation cannot be distinguished from the other processes at this stage, but it is expected to have a more prominent impact on grains of radius 1μm or larger, which are not included in our model.

To accommodate the boundary conditions of the MHD simulation, post-processing simulations were adjusted to allow outflows, but dust inflows are not included in PAPERBOATS so far. When considering inflows, the properties of incoming dust such as dust grain sizes, gas-to-dust mass ratio, and grain velocities are to be determined. If the inflow dust follows a MRN distribution and the gas-to-dust mass ratio is $\Delta_{gd} = 100$ at each time $t > 0$, then it is assumed that there was no dust destruction for the new inflowing dust grains, while there was dust destruction for the dust already present in the domain. Another aspect to take into account is the velocity of the inflowing dust. If the dust velocity is assumed to be the same as the gas, then this would imply that the dust is perfectly coupled to the gas, in contrast with the dust in the interiors.

5. Conclusions

We performed simulations of an SN blast wave expanding in a turbulent, magnetized ISM. Starting from a supernova-induced turbulent ISM, we obtained a high-resolution simulation and zoomed in on a high-density region. We then followed the evolution of a single SN, accumulating gas on its shock front and changing the dynamics of the already inhomogeneous medium. Through post-processing, we applied dust grains of several sizes to the background gaseous structure and computed the effects of the turbulence on the scattering, grain-to-grain collisions and vaporization of dust grains.

From the dust processing, we found that the SN had swept dust grains rapidly and that the dust mass being destroyed increased with the amount of dust initially present in the ISM. Due to the different gas and dust densities present in the region of SN injection, the results require further analysis as the fractional dust losses will give a more reliable comparison. In section 3.2 and 4, the importance of background processing of the ambient turbulent ISM is mentioned. The low speeds of the blast wave expansion restricted us from gaining a comprehensive view of the phenomenon. At high densities, it is therefore applicable to further increase the resolution and observe the phenomenon on a smaller scale. Further adjustments in the MHD simulation parameters, such as a smaller SN injection radius, need to be applied to allow comparison with similar simulations at a lower ISM density.

The effects of shocks in a magnetized high-density medium need to be explored further, as the unfolding of the dust budget crisis may play an important role in understanding how the dust components of galaxies evolve.

Code and software availability

The source code used for the simulations of this study, the PENCIL CODE (Pencil Code Collaboration 2021 [27]), is freely on https://github.com/pencil-code/. The updated re-meshing file will be committed to Github for general benefit. The PAPERBOATS code [28] is available upon reasonable request.

Acknowledgments

I would like to thank my supervisor Lars Mattson for his continuous guidance and encouragement. I recognize Frederick Gent for helpful discussions about the process of re-meshing and development of the simulations. The contribution of Florian Kirschlager by granting me the use of the software PAPERBOATS is gratefully acknowledged. I thank Axel Brandenburg for insightful comments and discussions inspiring this work. The simulations were performed using computational resources provided by the National Academic Infrastructure for Supercomputing in Sweden (NAISS) at the PDC Center for High Performance Computing, KTH Royal Institute of Technology in Stockholm.

References

[1] Brandenburg A and Subramanian K 2005 Astrophysical magnetic fields and nonlinear dynamo theory *Physics Reports* **417** 17

[2] Brandenburg A, Ntormousi E 2023 Galactic Dynamos. *ARA&A*. **61** 561-606

[3] Elmegreen BG, Scalo J 2004 Interstellar Turbulence I: Observations and Processes *ARA&A* 2004 **42** 211–273

[4] Williams DA. 2006 Gas and dust in the interstellar medium. *Journal of Physics* **6** 1

[5] Potapov A, McCoustra M 2021 Physics and Chemistry on the Surface of Cosmic Dust Grains: A Laboratory View

[6] Dominik C, Blum J, Cuzzi JN, Wurm G 2006 Growth of Dust as the Initial Step Toward Planet Formation

[7] McKee CF 1989 *Dust Destruction in the Interstellar Medium*. In: Allamandola LJ, Tielens AGGM, editors. Interstellar Dust. Springer Netherlands; 431-44

[8] Draine BT, McKee CF 1993 Theory of Interstellar Shocks *ARA&A* **31** 373-432

[9] Fry BJ, Fields BD, Ellis, R J 2020 Magnetic Imprisonment of Dusty Pinballs by a Supernova Remnant *The Astrophysical Journal* **894** 109

[10] Draine BT, Salpeter EE 1979 Destruction mechanisms for interstellar dust *ApJ* **231** 438-55
[11] Gent FA, Mac Low MM, Kapyla MJ, Singh NK 2021 Small-scale Dynamo in Supernova-driven Interstellar Turbulence *The Astrophysical Journal Letters* **910**
[12] Jones A, Tielens A, Hollenbach D 1996 Grain shattering in shocks: The interstellar grain size distribution. *Astrophysical Journal* **469** 740
[13] Borkowski KJ, Dwek E 1995 The Fragmentation and Vaporization of Dust in Grain-Grain Collisions *ApJ* **454** 254
[14] Bocchio, M , Jones, A P , Slavin, J D 2014 A re-evaluation of dust processing in supernova shock waves *AA* **570** A32
[15] Slavin JD, Dwek E, Jones AP 2015 Destruction of interstellar dust in evolving supernova remnant shock waves *The Astrophysical Journal* **803** 7
[16] Whittet DCB 2022 *Dust in the Galactic Environment* (Third Edition)
[17] Jones A, Tielens A, Hollenbach D, McKee C 1994 Grain destruction in shocks in the interstellar medium *Astrophysical Journal* **433** 797-810
[18] Kirchschlager F, Barlow MJ, Schmidt FD 2020 Silicate Grain Growth due to Ion Trapping in Oxygen-rich Supernova Remnants like Cassiopeia A *The Astrophysical Journal* **893** 70.
[19] Jones AP, Nuth JA 2011 Dust destruction in the ISM: re-evaluation of dust lifetimes *Astronomy and Astrophysics* **530**
[20] Mattsson L 2011 Dust in the early Universe: Evidence for non-stellar dust production or observational errors? *Monthly Notices of The Royal Astronomical Society* **414**
[21] Rowlands K, Gomez HL, Dunne L, Aragon-Salamanca A, Dye S, Maddox S, et al. 2014 The dust budget crisis in high-redshift submillimetre galaxiesm *MNRAS* **441** 1040-58
[22] Iffrig, O Hennebelle, P 2015 Mutual influence of supernovae and molecular clouds *AA* **576** A95
[23] Draine BT. 2011 *Physics of the Interstellar and Intergalactic Medium*
[24] Kirchschlager F, Mattsson L, Gent F 2021 Supernova induced processing of interstellar dust: impact of interstellar medium gas density and gas turbulence *MNRAS* **509** 3218-34
[25] Moseley ER, Teyssier R, Draine BT 2022 Dust dynamics in ramses – I. Methods and turbulent acceleration *MNRAS* **518** 2825–2844
[26] Kirchschlager F, Gent FA, Mattsson L 2023 Supernova dust destruction in the magnetized turbulent ISM (*Preprint)*
[27] Brandenburg A, Johansen A, Bourdin P, Dobler W, Lyra W, et al. 2021 The Pencil Code, a modular MPI code for partial differential equations and particles: multipurpose and multiuser-maintained *Journal of Open Source Software* **6** 2807
[28] Kirchschlager F, Schmidt FD, Barlow MJ, Fogerty EL, Bevan A, Priestley FD 2019 Dust survival rates in clumps passing through the Cas A reverse shock – I. Results for a range of clump densities *MNRAS* **489** 4465-96
[29] Brandenburg A, Dobler W 2002 Hydromagnetic turbulence in computer simulations *Computer Physics Communications* **147** 471-5
[30] Li M, Ostriker JP, Cen R, Bryan GL, Naab T. 2015 Supernova feedback and the hot gas filling fraction of the interstellar medium *The Astrophysical Journal* **814** 4
[31] Gent FA, Shukurov A, Fletcher A, Sarson GR, Mantere MJ 2013 The supernova-regulated ISM – I. The multiphase structure *MNRAS* **432** 1396–1423
[32] Wolfire M, Hollenbach D, Mckee C, Tielens A, Bakes E 1995 The neutral atomic phases of the interstellar medium *The Astrophysical Journal* **11** 443
[33] Sedov LI. 1960 Similarity and Dimensional Methods in Mechanics
[34] Bohlin RC, Savage BD, Drake JF 1978 A survey of interstellar H I from Lalpha absorption measurements II *ApJ*. **224** 132-42
[35] Mathis JS, Rumpl W, Nordsieck KH 1977 The size distribution of interstellar grains *ApJ*. **217** 425-33
[36] Hu C, Zhukovska S, Somerville RS, Naab T 2019 Thermal and non-thermal dust sputtering in hydrodynamical simulations of the multiphase interstellar medium *MNRAS* **487** 3252-69

[37] Gent FA, Shukurov A, Sarson GR, Fletcher A, Mantere MJ 2012 The supernova-regulated ISM – II. The mean magnetic field. *MNRAS* **430** L40–L44
[38] Brandenburg A, Korpi MJ, Mee AJ. 2007 Thermal Instability in Shearing and Periodic Turbulence *ApJ* **654** 945-54
[39] Kim CG, Ostriker EC 2015 Momentum Injection by Supernovae in the Interstellar Medium *ApJ* **802** 99
[40] Mattsson L, De Cia A, Andersen AC, Zafar T 2014 On the (in)variance of the dust-to-metals ratio in galaxies *MNRAS* **440** 1562-70
[41] Kirchschlager F, Schmidt FD, Barlow MJ, De Looze I, Sartorio NS 2023 Dust survival rates in clumps passing through the Cas A reverse shock - II. The impact of magnetic field *MNRAS* **520** 5042-64